COMBINING DIGITAL IMAGE CORRELATION, PASSIVE THERMOGRAPHY AND ACOUSTIC EMISSION TO INVESTIGATE DAMAGE INITIATION AND PROPAGATION OF OUT-OF-PLANE FIBER WAVINESS

M. Thor[1,3,a], H. Plasser[2,b], M. Nagler[1,c], F. Maier[1,d], R. M. Hinterhölzl[1,e] and M. G. R. Sause[3,f]

[1] Research Group of Lightweight Design and Composite Materials, University of Applied Sciences Upper Austria, Stelzhamerstraße 23, 4600 Wels, Austria, https://www.fh-ooe.at/en/
[2] Josef Ressel Center for Thermal NDE of Composites, University of Applied Sciences Upper Austria, Stelzhamerstraße 23, 4600 Wels, Austria, https://www.thermo-ndt.at/
[3] Institute of Materials Resource Management, University of Augsburg, Universitätsstraße 1 Nord, 86159 Augsburg, Germany, http://www.mrm.uni-augsburg.de/en/

[a] michael.thor@fh-wels.at, [b] holger.plasser@fh-wels.at, [c] michaela.nagler@fh-wels.at, [d] franz.maier@fh-wels.at, [e] roland.hinterhoelzl@fh-wels.at, [f] markus.sause@mrm.uni-augsburg.de,

Keywords*: Composite materials, Fiber waviness, Digital image correlation, Passive thermography, Acoustic emission

ABSTRACT

The currently limited capability to predict material failure in composite materials in general and in wavy composite layers specifically has led to high margins of safety for the design of composite structures. Thus, the full lightweight potential of this class of materials is left unused. To understand the complex failure behaviour of composite materials containing out-of-plane fiber waviness under compressive and tensile loading, digital image correlation, passive thermography and acoustic emission test methods are used to investigate damage initiation and propagation on specimen level. These methods deliver qualitative trends as well as quantitative metrics about the damage behavior in wavy CFRP materials. This data can be further used in constitutive laws to gain deeper insight and understanding in the material behavior.

1 INTRODUCTION

Out-of-plane fiber waviness is a common effect inherent to various manufacturing processes of fiber-reinforced composite parts. They cannot be completely avoided and therefore have to be tolerated and be considered as an inherent part of the structure. To this point, there is still no acceptable approach to quantitatively support accept/reject/repair-decisions and make a consistent assessment of wavy layers in composites. Fiber misalignments in general are known to have a detrimental effect on the compressive strength of composite materials. To investigate these effects, the damage initiation and propagation is investigated in this work by tensile and compression tests accompanied by experimental test methods such as digital image correlation (DIC), passive infrared thermography (IRT) and acoustic emission (AE).

2 MATERIALS AND METHODS

2.1 Specimen preparation

A pre-impregnated polymer composite consisting of IM7 unidirectional carbon fiber reinforcement embedded in a 8552 thermosetting epoxy matrix (Hexcel Corporation) is used. The nominal cured ply thickness of the UD prepreg layer is 0.131 mm according to the material data sheet. The laminates are fabricated in an autoclave according to the curing cycle for monolithic components. Planar reference specimen thickness is kept at 2.1 mm following test standards. For the unidirectional (UD) laminate 16 layers oriented in 0° and for the quasi-isotropic (QI) laminate 16 layers in total with a stacking sequence of $(0/45/-45/90)_{2s}$ were used. The thickness of both the UD and QI laminate including different types of sinusoidal waves was realized by 40 plies in 0° and a stacking sequence of (0/45/-

45/90)$_{5s}$ respectively, leading to a laminate thickness of ~5.1 mm. Two wave configurations were realized with a wavelength L_1=27.9 mm and amplitude A_1=1.19 mm (wave 1) and L_2=14.5 mm and A_2=0.58 mm (wave 2).

2.2 Experimental methods and test set-ups

2.2.1 Tensile and compression testing

Tensile and compression tests are carried out in the spirit of ASTM D3039 and ASTM D6641. Material testing was conducted on universal test machines from Zwick and Messphysik with a maximum load of 150 kN and 250 kN respectively. Specimens were loaded at a rate of 1 mm/s. Coupling the DIC, IRT and AE measurement systems with the test machine via analog inputs allows for a simultaneous recording of images with the corresponding force and displacement signal. The conducted tests on wavy specimens are summarized in the following test matrix. An extensive material characterization on planar specimens was also performed, but is outside the scope of this paper.

	Digital image correlation	Passive thermography	Acoustic emission
Wave 1 UD compression	6	4	
Wave 2 UD compression	6	4	
Wave 1 UD tension	6	4	
Wave 1 QI tension	8		8

Table 1: Test plan (configurations and number of specimens)

2.2.2 Digital image correlation

Digital image correlation (DIC) is a powerful tool for measuring strain distributions during mechanical testing of materials. In contrast to traditional extensometers or applied strain gauges, with a typical gauge length of several tens of millimetres, DIC delivers full-field information of the strain state for each load step. In general, DIC is based on the principle of comparing stochastic distributed speckle patterns of the undeformed reference state to any deformed state. For the strain analysis, a virtual grid of subsets (facets) is overlaid on the applied speckle pattern. The deformation during the loading process is recorded with a camera system and the subsets are tracked by the software. The in-plane strain distribution on the surface of the specimen is gained without a priori knowledge of the constitutive behaviour. When observing materials with a non-uniform microstructure and a resulting non-uniform local loading condition, like it is present in the behaviour of out-of-plane fiber waviness with a complex strain field, a full-field strain measurement is necessary. In recent years, several studies on composite materials have been performed using DIC [1-2], also specifically on the investigation of fiber waviness in composites [3-4]. In the present study, the full-field through-thickness strain distribution was measured with a GOM Aramis 3D 12M DIC system. Depending on the required field of view 50 mm and 100 mm lenses were used and a homogeneously distributed speckle pattern was applied on a matt white grounding using an airbrush system. Images were obtained at 10 Hz. The test-set up is shown in Fig. 1.
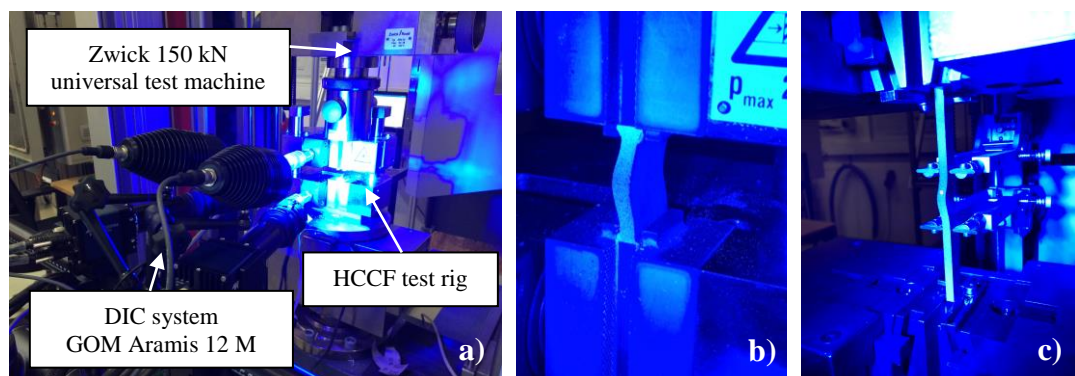

Figure 1: a) DIC test set-up; b) compression specimen; c) tensile specimen.

2.2.3 Passive infrared thermography

In passive thermographic methods, the temperature distribution of the test object is monitored as resulting from its regular operation. In the case of applied mechanical loads, damage events occur and dissipate heat allowing their localisation. In this study, a passive thermographic approach was used to locate the failure initiation and propagation by using a high-resolution infrared (IR) camera FLIR X8400sc equipped with an indium antimonide (InSb) detector. The cooled 1280 x 1024 pixel focal plane array camera has a noise equivalent temperature difference (NETD) of about 25 mK and is sensitive in a spectral range of 1.5 to 5.1 micron. The measurements were carried out with a frame rate of 172 Hz and an approximate spatial resolution of 70 µm. The field of view was set to be consistent with the strain field measurements. The test set-up for passive thermography is shown in Fig. 2.

Figure 2: Passive thermography test set-up for tensile test.

2.2.4 Acoustic emission

The rapid microscopic displacements caused by microscopic failure mechanisms in fiber-reinforced composite materials cause an excitation of elastic waves in the ultrasonic frequency range. These transient acoustic signals can be detected and analysed using piezoelectric sensor systems. The measured acoustic emission signals can be used to detect the onset and position of microscopic failure events occurring in fiber-reinforced composite materials. [5-11]

In recent years, many attempts [6-10, 12] have been made to distinguish between different types of failures such as fiber breakage, matrix cracking and interfacial failure in fiber-reinforced materials. The analysis of the measured acoustic emission signals used in the present study is based on previous work [13,14]. It follows a recently developed pattern recognition method [15] to distinguish and quantify the above mentioned failure mechanisms in carbon fiber-reinforced polymers. The validity of the source identification by the proposed method is based on reference calculations [16-18] of the acoustic emission source, signal propagation, and signal detection process by finite element modelling.

Two wide band (WD) AE sensors were attached in linear arrangement at opposing ends of the specimen as illustrated in Fig. 3 and Fig. 4. In the present case, the AE test method is only used for the tensile specimens due to space limitations of the low free length in compression. AE tests are conducted on wavy as well as on flat reference tensile specimen. AE signals were acquired using a Mistras PCI-2 system with 2/4/6 preamplifiers. A threshold-based triggering mechanism using 10/80/300 µs (Peak-Definition-Time/Hit-Definition-Time/Hit-Lockout-Time) at a threshold of 35 dB$_{AE}$ and a preamplification of 20 dB$_{AE}$ was used. The data were recorded with an acquisition rate of 10 MSP/s and a band-pass filter ranging from 20 kHz to 1 MHz using the software AEwin. An Event-Definition-Time filter of (15±2) µs was used to detect only signals from source positions located in the range between the two sensors. A medium viscosity silicone grease (KORASILON™, Kurt Obermeier, Germany) was used to provide an adequate acoustic coupling. The sensors were attached to the specimen using standard clamp systems, shown in Fig. 4, to ensure a reproducible mounting pressure. The sensor coupling was validated by mutual pulsing of both sensors and comparison of the detected signal amplitudes in an automatic sensor test (AST). The sound velocity of the initial arrival of the Lamb wave is obtained from the measured time difference between the time of pulsing of sensor 1 and the arrival time at sensor 2 divided by their respective metric distance (118 ± 1 mm for both wavy and plane reference specimens). A pencil lead break test (PLB) was carried out

according to ASTM E976 for each specimen before testing. This technique, named Hsu-Nielsen source after its developers, simulates an acoustic emission event by breaking a brittle graphite pencil lead with a diameter of 0.5 mm, located in a suitable fitting, approximately 3 mm (± 0.5 mm) away from its tip by pressing it against the surface of the specimen. This intense artificial acoustic signal simulates a very loud out-of-plane acoustic emission source. This test ensures that the transducers are in good acoustic contact with the specimen being monitored and also checks the accuracy of the source location setup. In addition to the above mentioned tests, signals are measured for approximately one minute with the mechanical measuring system completely at rest before the actual test is carried out. This is done to ensure, that signals, generated outside the measurement area are not recorded. After signal acquisition from mechanical testing, the acoustic emission source position was calculated by Δt-localization techniques using the one-dimensional sensor arrangement. Only localized signals that fulfil the condition $\left| \Delta t \right| \leq 20$ µs, were taken into account for further analysis. An application of the pattern recognition method described in [15] yields three signal classes for all eight plane reference and eight wavy specimens investigated. For the pattern recognition method, the acoustic emission signal features of both sensors were calculated from the first 200 µs of the signals after the signal arrival.
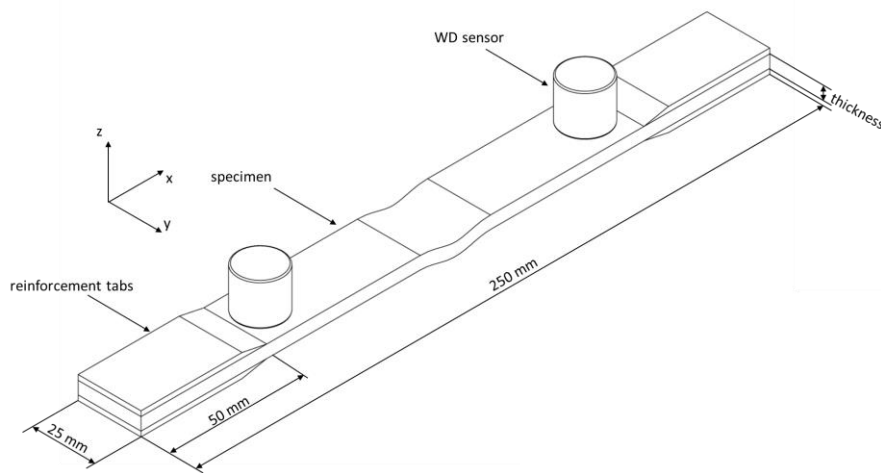

Figure 3: Wavy specimen dimensions and linear arrangement of the acoustic emission sensors.
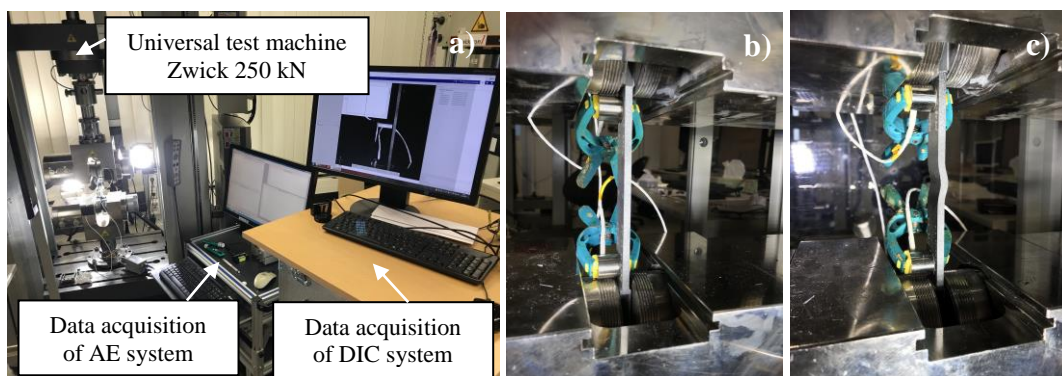

Figure 4: a) Acoustic emission test set-up; b) planar reference specimen; c) wavy specimen.

3 RESULTS AND DISCUSSION

3.1 Digital image correlation

The applied unidirectional load leads to a complex 2D strain state at the observed cross-section due to the presence of the wave. In Fig. 5 the shear strain ε_{xy} distributions of wavy specimens are shown before and after final damage within two frames (10 Hz) for a) wave 1 and b) wave 2 under compression and c) wave 1 under tensile load. Regions of high strain coincide well with the

occurrence of macroscopic material failure. The associated shear stress τ_{13} is, according to [19], the most significant stress component for wavy composites under axial compression. Higher amplitudes (A ↑) and lower specimen thicknesses (t ↓) lead to higher bending moments with a maximum in the longitudinal centre of the wave, which leads to bending stresses. These in turn superpose with the global compressive or tensile load. This mechanism in form of variations of the longitudinal strain component ε_x is schematically shown in Fig. 6 and 7.
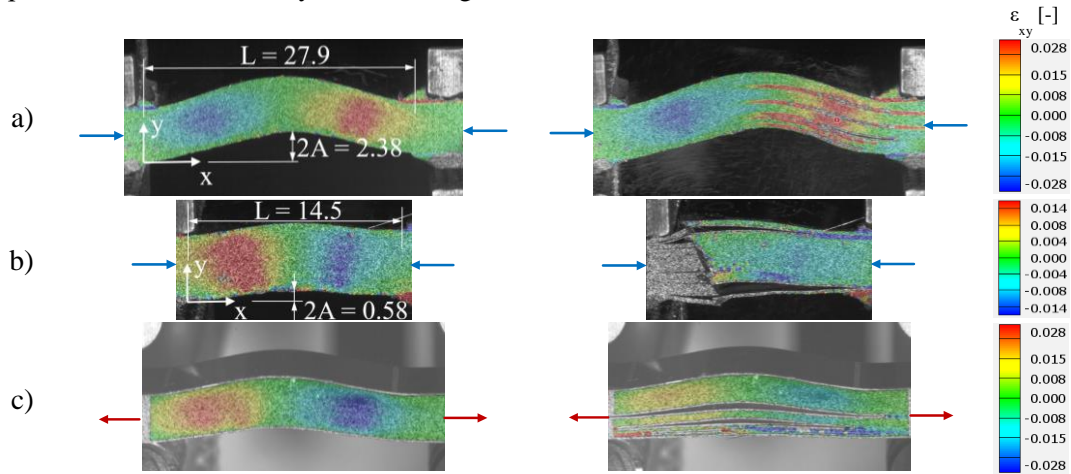
Figure 5: Shear strain ε_{xy} distribution in the frame captured right before and after macroscopic damage for UD specimen configurations
a) wave 1 in compression; b) wave 2 in compression; c) wave 1 in tension.

There is a transition from tension to compression of ε_x in thickness direction when global compression and tension is applied (Fig. 6). Wave 2 (less pronounced waviness) shows a gradient in the strain component but no change from tensile to compression strains. This difference can be described as structural level (wave 1) and material level (wave 2) influenced mechanical properties of the wave. This influence on a structural level is amplified during compression testing due to an increasing amplitude-to-wavelength ratio (A/L).
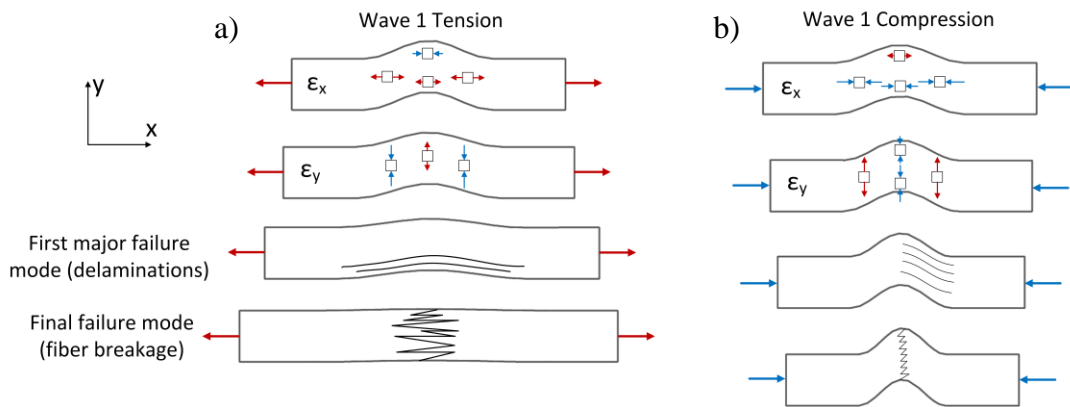

Figure 6: Schematic illustration of damage behavior of wave 1 specimens under tensile and compression load including normal strains ε_x and ε_y.

In addition to the above mentioned shear strains that are significantly influencing the failure behaviour, tensile strains, respectively stresses in thickness direction potentially cause the individual layers to lift off in form of delamination, as shown in Fig. 6. This leads to the conclusion, that the resulting stresses superpose with shear stress components and also significantly influence the failure behaviour. In global tensile loading (Fig. 6 a)), the resulting through thickness strain component ε_y in wave 1 shows a maximum in tension at the center of the wave leading to delamination along the whole wave length, initiated at the wave center. Wave 2 shows a maximum tensile strain component ε_y at the

turning point of the sinusoidal wave under compression loading. This leads to one-sided delamination initiated at the area of maximum inclination of the sine wave.
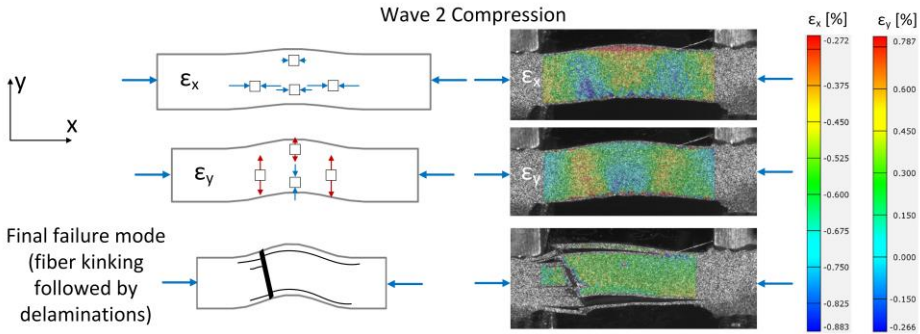

Figure 7: Schematic illustration and corresponding DIC results of damage behavior of wave 2 specimens under compression load including normal strains ε_x and ε_y.

Global compression load of wave 2 and the absence of notable bending moments leads to fiber kinking of the specimen schematically depicted in Fig. 7. The positive strain ε_y in thickness direction leads to less supported fibers and therefore promote the appearance of kink bands. These results suggest, that the failure of wave 1 is influenced by the effect of the geometry in form of resulting bending moments in contrast to wave 2 where the failure behavior is more determined by the material.

3.2 Passive thermography

In-situ passive thermography is used to assess the damage initiation and propagation during quasi-static mechanical loading in compression and tension. Representative images obtained during mechanical testing are shown in Fig. 9 (wave 1 in compression), Fig. 10 (wave 2 in compression) and Fig. 11 (wave 1 in tension). Damage initiation was visible as clear bright spots and the progressing delamination appeared as a bright line. Due to a higher energy release of fiber bundle failure in comparison to the lower energy releases of matrix failure, the type of damage can be clearly identified by single point evaluations of the resulting peak values of thermal intensities as shown in Fig. 8. The p-value < 0.0002, resulting from a one-way ANOVA, determines that the differences between the group means of matrix and fiber bundle failure are statistically significant. The presented digital levels (thermal intensities) of the IR quantum detector are a metric directly related to the temperature. Fiber bundle failure results in approximately two times higher thermal intensities than matrix failure. Clustering these results of (near-)surface damage events on macroscopic level gives the opportunity to distinguish results on smaller scales, e.g. single fiber breakage or small matrix cracks.
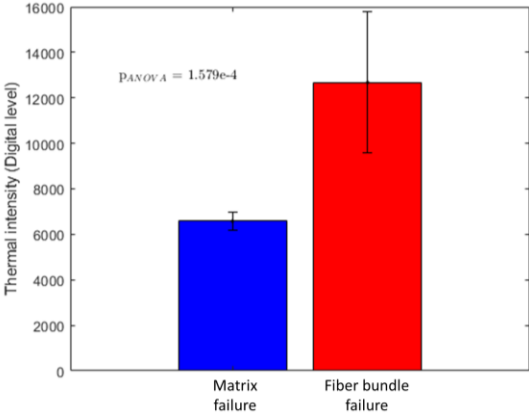

Figure 8: Thermal intensities (digital levels) of first major damage events.
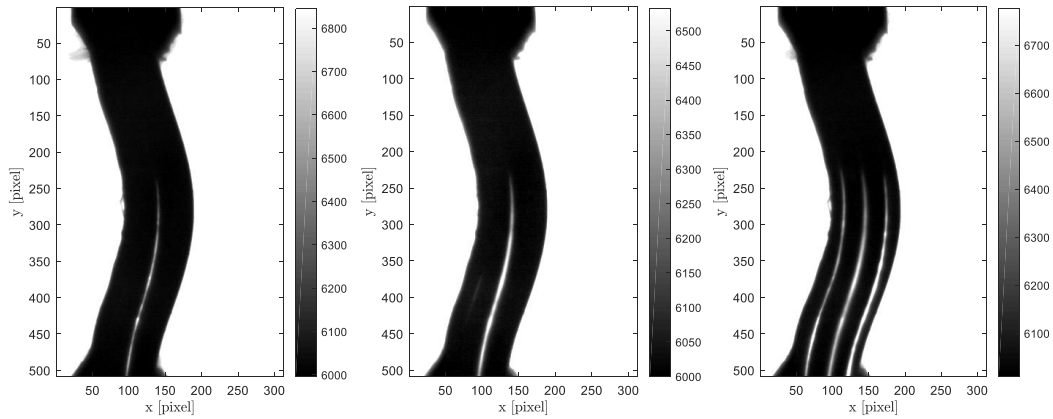
Figure 9: Thermal intensity (digital level) images from IRT of compression test on wave 1 specimen with UD-laminate.
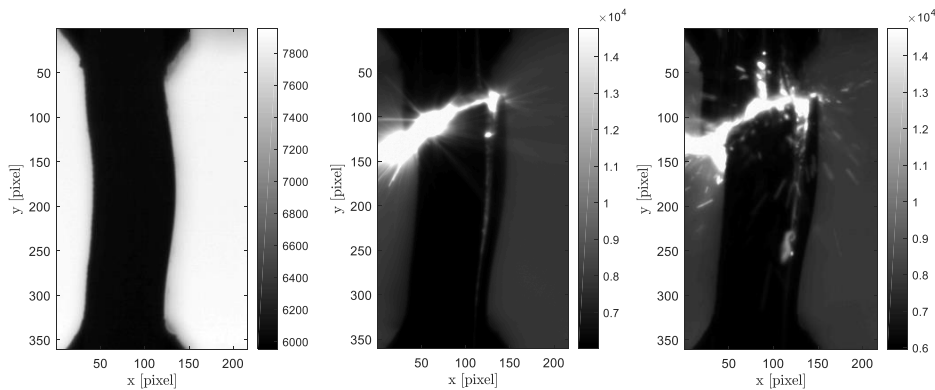

Figure 10: Thermal intensity (digital level) images from IRT of compression test on wave 2 specimen with UD-laminate.
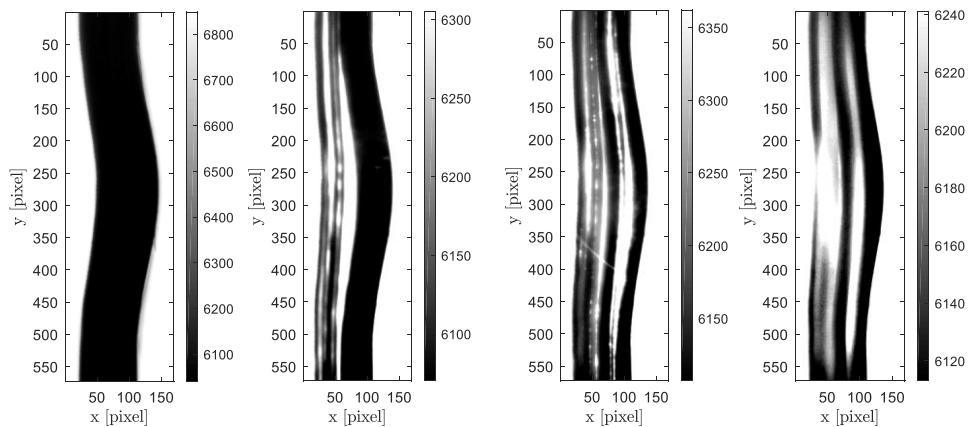

Figure 11: Thermal intensity (digital level) images from IRT of tensile test on wave 1 specimen with UD-laminate.

In Fig. 12, a representative result of the averaged thermal intensity associated with the IRT results shown in Fig. 9, is shown with the corresponding compression force. The disadvantage of averaging the thermal intensities over the region of interest (wavy region) is that individual failure modes cannot be identified but a general thermal response under mechanical loading can be investigated. Zone 1 is characterized by an almost linear increase of the elastic material response to the external load. In zone

2, a clear increase in intensities indicate the presence of micro-cracks. The increase of micro-cracks can be also observed in a reduced slope of the force signal. The three delamination, shown in Fig. 9, appear within three frames with a frame rate of 172 Hz (sample time ~17.4 ms) representing the sudden transition from zone 2 to zone 3, leading to a strong increase in temperature and drop of compression force.
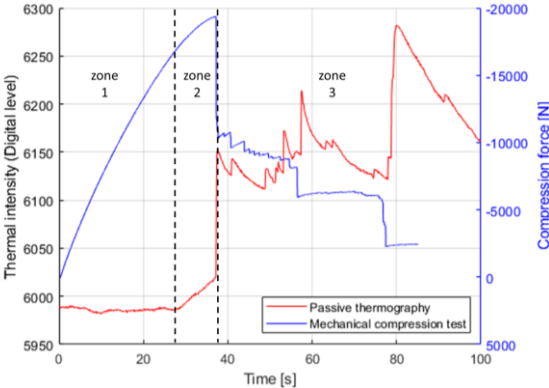

Figure 12: Force-displacement curve and corresponding thermal intensities from IRT of compression test on wave 1 specimen with UD-laminate.
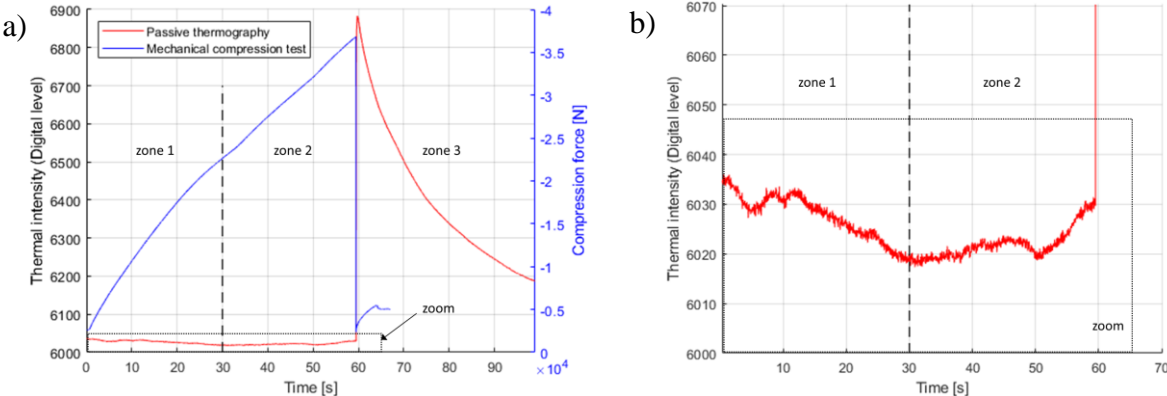

Figure 13: a) Force-displacement curve and corresponding thermal intensities from IRT of compression test on wave 2 specimen with UD-laminate;
b) Detail of thermal intensity change in zone 1 and zone 2.

The thermo-mechanical behavior [21, 22], where the mechanical energy of testing is completely stored in the material, was observed in the tests. The specimens show an approximately linear decrease in temperature in the initial elastic region (zone 1) as depicted in the zoomed region in Fig. 13 (b). The transition from the elastic region zone 1 to zone 2 constitutes a significant decrease in stiffness until final failure in form of fiber kinking occurs. The high energy that is dissipated in fiber kinking is not plotted in Fig. 13 as the depicted results are averaged over the wavy region of the specimen as described above and therefore just illustrates a qualitative picture of the damage behavior. A single point evaluation of various damage events is shown in Fig. 8.

The small peaks in thermal intensities, depicted in Fig. 14, correspond to delamination (Fig. 11) in tensile tests. The first two deflections in the force signal are due to damages in the clamping area, which was outside the field of view of the IR camera.
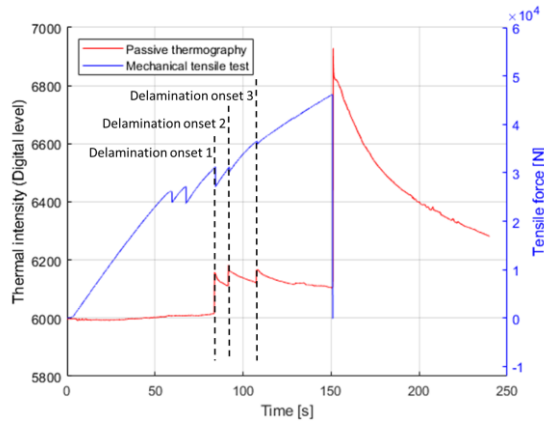
Figure 14: Force-displacement curve and corresponding thermal intensities from IRT of tensile test on wave 1 specimen with UD-laminate.

3.3 Acoustic emission

AE is used to localize damage initiation and to distinguish between fiber and matrix failure in quasi-isotropic tensile specimen with wave 1 (more pronounced waviness) configuration. The density plot (Fig. 15) of damage events clearly shows localized areas in the wavy regions. Matrix cracking in 90° and ±45° plies is evenly distributed along the specimen length with a slightly more dense distribution in the wavy region. AE confirmed that the wavy region is more prone to delamination in tension as well as in compression consistent with DIC and IRT results.
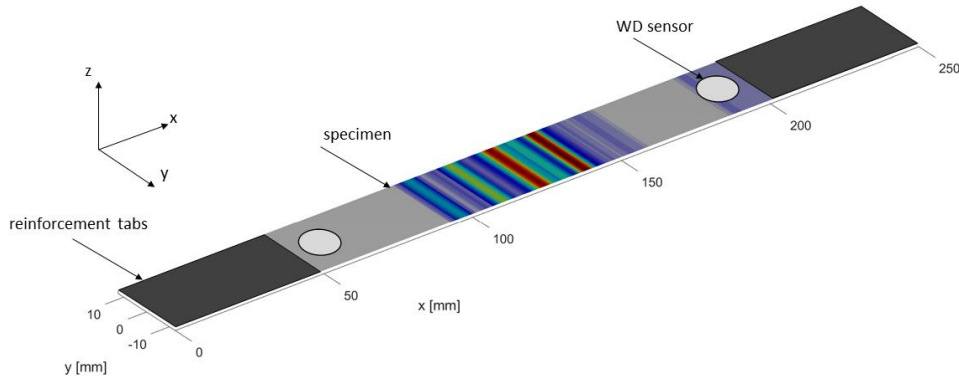

Figure 15: Representative density plot of acoustic emission results with weighting of absolute energy for wavy specimen projected on flat surface.
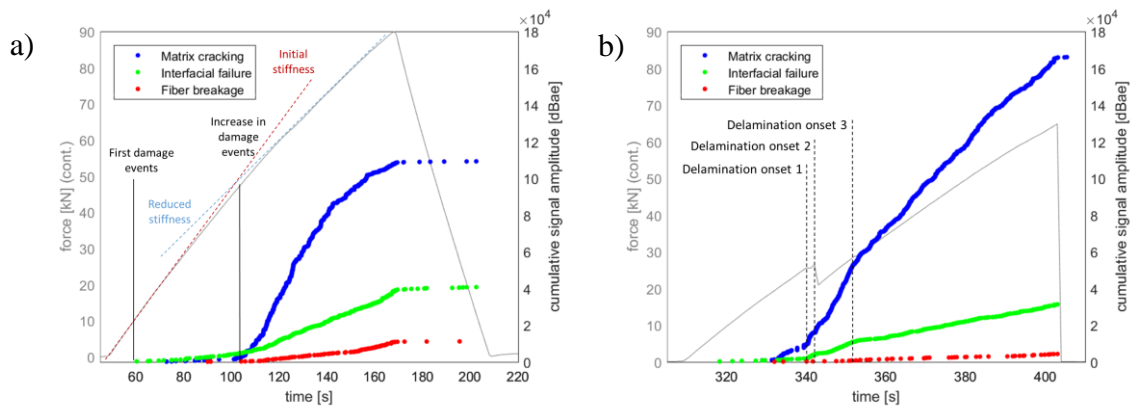

Figure 16: Force and cumulative signal amplitude over time results of acoustic emission testing for a) planar reference specimen and b) wavy specimen.

The reduction of stiffness in plane reference results (Fig. 16, a) coincides well with the major increase in damage events. The increase in matrix cracking and interfacial failure after major delamination in wavy specimens (Fig. 16, b) can be explained by changes in load paths. The resulting lack of load transmission in failed layers must be compensated by other layers, which have not yet failed. This abrupt increase in load leads to an increasing rate of matrix cracking.
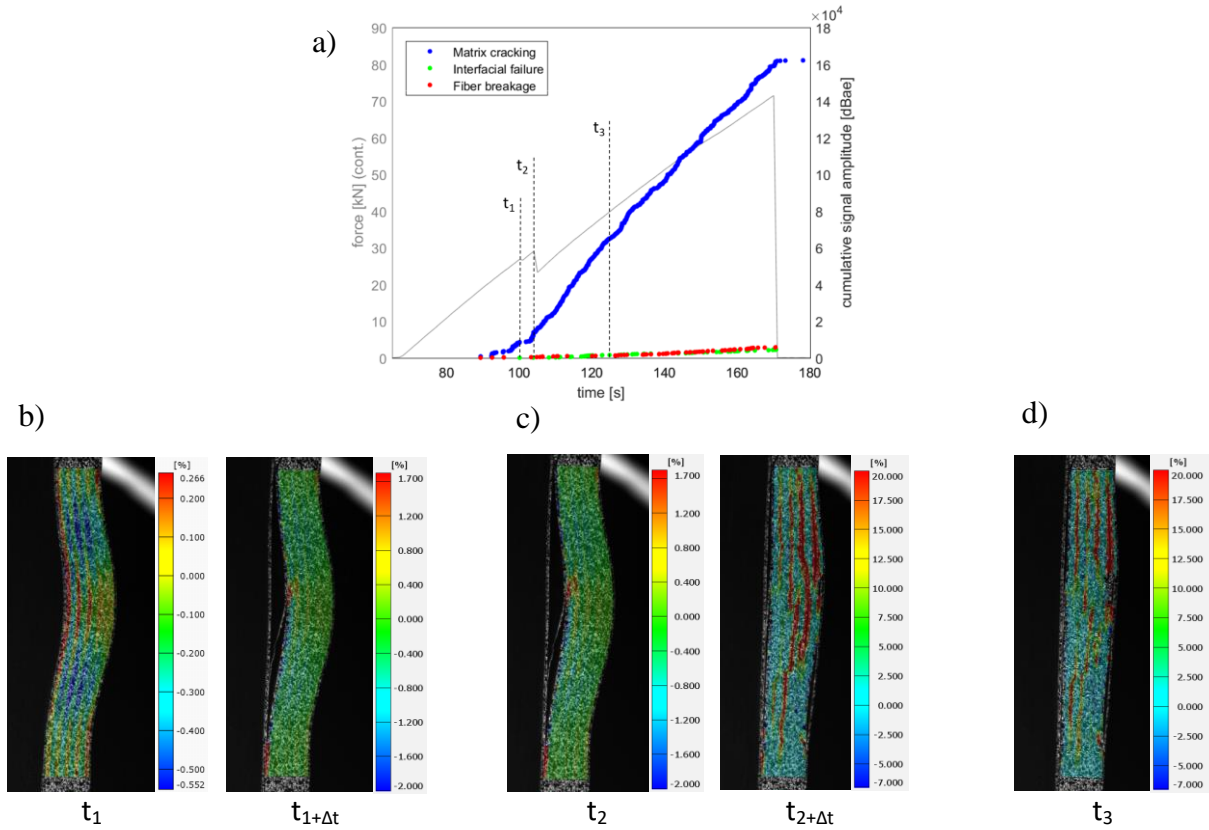

Figure 17: Cumulated signal amplitude over time results of acoustic emission testing (a) and comparison with DIC results ε_y obtained from wavy specimen (b-d).

Existing delamination, shown in Fig. 17, are closing due to the straightening of the wave, but no increase in stiffness can be observed for quasi-isotropic specimen. Because of this closing mechanism, it is difficult to follow delamination during the whole loading process. The area of delamination appears to be larger in frame t_2 than in frame t_3, where Δt indicates the subsequent frame of the shown DIC results.

3.4 Assessment of test methods

A summarized assessment of the considered test methods is presented in Table 2.

	Digital image correlation	Passive thermography	Acoustic emission
Damage localization method	Optical	Optical	Arrival time of signals
Damage distinction method	Optical distinction of damage modes based on strain signatures	Optical distinction of damage modes based on thermal intensity signatures	Classification based on frequency and intensity of AE signals
Matrix cracking	Good, but strongly dependent on the field of view and the resulting resolution	Good	Good

Delamination	Good	Good	Good
Fiber breakage	Fiber bundles (Good); Single fiber breakage (Difficult)	Good, but depending on the resolution	Good
Local loading condition	Strain field (Very good)	No information, except thermo-mechanical effect	No information
Inspection level	Surface	Surface and near surface damages	Entire Volume
Test part sizes	Small (mm) to large (m) → with <u>major</u> losses of damage event information on larger scales	Small (mm) to large (m) → with <u>minor</u> losses of damage event information on larger scales	Small (cm) to large (m) → <u>no</u> information loss because of the possibility to use more sensors
Uncertainty in evaluation of signals	Low	Low to medium	Medium

Table 2: Assessment of test methods

4 CONCLUSIONS AND OUTLOOK

The knowledge of intrinsic material behavior of fiber reinforced composite materials on microscopic level up to macroscopic or structural level is of crucial importance for the development of suitable material laws for numerical modeling and for a deeper understanding of deformation and damage mechanisms. The described combination of experiments was able to capture composite material failure in great detail. Inhomogeneous deformations observed in out-of-plane fiber waviness cannot be adequately recorded by traditional extensometers. DIC provides information on mechanisms and a full 2D strain field prior to failure, e.g. the location of strain concentrations. However, capturing damage initiation is limited by the (typically lower) frame-rate as well as the detectable size of an event. Both of which are compensated by passive thermography. Passive thermography signals can be clearly matched with results from DIC and AE. While both methods are limited to the surface of the specimen, information of internal processes was obtained by AE. Specifically, the difference between matrix cracking, interfacial failure and fiber breakage was evident from differences in the acoustic emission signals. Overall, our results suggest that, depending on the laminate configuration (amplitude, wavelength, thickness) interlaminar shear failure is the dominant failure mechanism that is followed by mode I delamination and layer-wise buckling. For wave configurations with a lower amplitude-to-thickness ratio fiber kinking is the dominant failure mechanism under compression loading. The observed formation of a shear kink-band under compression and shear stress (Fig. 5 (b) DIC and Fig. 10 IRT) is caused by local fiber buckling which is induced by misaligned fibers in the UD materials that continue to rotate under load.

ACKNOWLEDGEMENTS

REFERENCES

[1] H. Koerber, J. Xavier, P.P. Camanho "High strain rate characterisation of unidirectional carbon-epoxy IM7-8552 in transverse compression and in-plane shear using digital image correlation". *Mech Mater*; 42:1004–19. 2010.

[2] M. Jerabek, Z. Major, R.W. Lang "Strain Determination of Polymeric Materials Using Digital Image Correlation". *Polymer Testing 29* (3): 407–16. 2010.

[3] A. Altmann, R. Taubert, U. Mandel, R.M. Hinterhölzl, and K. Drechsler "A Continuum Damage Model to Predict the Influence of Ply Waviness on Stiffness and Strength in Ultra-Thick

Unidirectional Fiber-Reinforced Plastics". *Journal of Composite Materials, Vol. 50(20), 2739-2755.* 2016.

[4] P. Davidson, M. Waas "Effect of Fiber Waviness on the Compressive Strength of Unidirectional Carbon Fiber Composites". 53rd AIAA/ASME/ASCE/AHS/ASC Structures, Structural Dynamics and Materials Conference, no. April: 1–16. 2012.

[5] M. Surgeon and M. Wevers "Modal analysis of acoustic emission signals from CFRP laminates". NDT & E Int; 32: 311–322. 1999.

[6] J. Bohse "Acoustic emission characteristics of microfailure processes in polymer blends and composites". Compos Sci Technol 2000; 60: 1213–1226.

[7] Haselbach Wand Lauke B. "Acoustic emission of debonding between fibre and matrix to evaluate local adhesion". Compos Sci Technol 2003; 63: 2155–2162.

[8] C.R. Ramirez-Jimenez, N. Papadakis, N. Reynolds, et al. "Identification of failure modes in glass/polypropylene composites by means of the primary frequency content of the acoustic emission event". Compos Sci Technol; 64: 1819–1827. 2004.

[9] A. Marec, J.H. Thomas and R. Guerjouma "Damage characterization of polymer-based composite materials: multivariable analysis and wavelet transform for clustering acoustic emission data". Mech Syst Signal Process; 22: 1441–1464. 2008.

[10] X. Li, C. Ramirez, E.L. Hines, et al. "Pattern recognition of fiber-reinforced plastic failure mechanism using computational intelligence techniques". In: Neural networks. IEEE world congress on computational intelligence, Hong Kong, pp.2340–2345. IEEE. 2008.

[11] V. Kostopoulos, P. Karapappas, T. Loutas, et al. „Interlaminar fracture toughness of carbon fibrereinforced polymer laminates with nano- and microfillers." Strain; 47: e269–e282. 2011.

[12] J.J. Scholey, P.D. Wilcox, M.R. Wisnom, et al. "Quantitative experimental measurements of matrix cracking and delamination using acoustic emission". Compos Part A: Appl Sci Manufact; 41: 612–623. 2010.

[13] M.G.R. Sause "In Situ Monitoring of Fiber-Reinforced Composites". Springer Series in Materials Science, Springer International Publishing, 2016.

[14] T. Prieß, M.G.R. Sause, D. Fischer, P. Middendorf "Detection of delamination onset in laser-cut carbon fiber transverse crack tension specimens using acoustic emission". *Journal of Composite Materials*, Vol. 49:21, pp 2639-2647, 2015.

[15] M.G.R. Sause, A. Gribov, A.R. Unwin et al. "Pattern recognition approach to identify natural clusters of acoustic emission signals". *Pattern Recogn Lett; 33: 17-23.* 2012.

[16] M.G.R. Sause, S. Horn "Simulation of acoustic emission in planar carbon fiber reinforced plastic specimens" *J Nondestr Eval*; 29: 123-142, 2010.

[17] M.G.R. Sause, S. Horn "Influence of specimen geometry on acoustic emission signals in fiber reinforced composites: FEM-simulations and experiments. In: *Proceedings of the 29th European conference on acoustic emission*, Vienna, Austria, 2010.

[18] M.G.R. Sause, T. Müller, A. Horoschenkoff et al. „Quantification of failure mechanisms in mode-I loading of fiber reinforced plastics utilizing acoustic emission analysis". *Compos Sci Technol*; 72: 167-174. 2012.

[19] H.M. Hsiao and I.M. Daniel "Elastic properties of composites with fiber waviness". *Composites Part A: Applied Science and Manufacturing*, Vol. 27, Issue 10, pp 931-941, 1996.

[20] M.G.R. Sause, S. Horn "Quantification of the uncertainty of pattern recognition approaches applied to acoustic emission signals. J Nondestr Eval; 32: 242-255. 2013

[21] W. Harizi, S. Chaki, G. Bourse, M. Ourak "Mechanical damage assessment of Glass Fiber-Reinforced Polymer composites using passive infrared thermography". *Composites: Part B,* Vol. 59: 74-79. 2014.

[22] F. Libonati, L. Vergani "Damage assessment of composite materials by means of thermographic analyses". *Composites: Part B*, Vol. 50: 82-90. 2013.